Stability Analysis of Profile Following by a CDPR using Distance and Vision Sensors*

Thomas Rousseau[1,2][0000−0001−9939−9688], Nicolò Pedemonte[2][0000−0002−4811−3907], Stéphane Caro[1][0000−0002−8736−7870], and François Chaumette[3][0000−0002−1238−4385]

[1] Nantes Université, Ecole Centrale Nantes, CNRS, LS2N, UMR 6004, Nantes, France thomas.rousseau@ls2n.fr, Stephane.Caro@ls2n.fr
[2] IRT Jules Verne, Bouguenais, France nicolo.pedemonte@irt-jules-verne.fr
[3] Inria, Univ Rennes, CNRS, IRISA, Rennes, France Francois.Chaumette@inria.fr

Abstract. Cable-Driven Parallel Robots (CDPRs) form a class of robots well-adapted to large workspaces since they replace rigid links by cables. However, they lack in positioning accuracy. In a previous work, a control law has been proposed to enable a CDPR to perform a profile-following task, based on the data measured by two different and redundant sensors that are fused using the Gradient Projection Method (GPM). However, its robustness had not been assessed yet. This paper analyzes the stability of such a control law in function of the systematic errors on the parameters of the system. Numerical simulations show that the characteristics of the system ensure the stability of the control law in the robot workspace even in the presence of significant errors, provided the initial angle between the surface to follow and the moving-platform is smaller than 11°.

Keywords: Stability Analysis · Sensor-based control · Cable-Driven Parallel Robot

1 Introduction

Cable-driven parallel robots (CDPRs) are robots where the end-effector, named the moving-platform (MP), is actuated by a set of cables instead of rigid links. The length of the cables is usually controlled by a drum-pulley system, actuated by motors fixed to the main frame. These robots are able to carry loads in large workspaces and could thus help in large industrial assembly tasks. However, their accuracy, especially for positioning with regards to a given object, needs to be improved before they can find a place on production lines. While many research works brought significant improvements to CDPR models [1–3], sensor-based control, and especially vision-based control [4–6], can also enable such robots to reach a better precision, without needing the tedious computations required for the Forward Kinematics.

* This work is supported by IRT Jules Verne in the framework of the PERFORM program.

However, vision-based control has some important limitations: embedded cameras suffer from a limited field of view, while external cameras provide a global overview of the workspace but at the cost of worse accuracy. A solution to these shortcomings was proposed in [7] where measurements from both distance sensors and an external camera are combined using the Gradient Projection Method (GPM) [8, 9] to prioritize tasks. The robustness of this control law was not considered in [7]. While the stability analysis for N-tasks problems was investigated in [10], the proposed stability criterion is only valid in the ideal case while a specific study based on the quality of the estimations and possible sensor biases is required in our case. The robustness of CDPR control for one pure visual task has been tackled in [5]. A novel workspace named Control Stability Workspace (CSW), enclosing the stable poses for given perturbation bounds, was also introduced in [11].

In this paper, the robustness of the GPM control for a profile following task is assessed. First, a stability criterion is derived from the control law of the system. Then, the impact on stability of all the identified error sources is investigated. Finally, a combined analysis is run in the robot operating conditions to confirm its robustness. Since experimental results have already been presented in [7], only simulation results are discussed in this paper. A view of the experimental platform used in this paper, ACROBOT, a six degrees of freedom (DoF) suspended CDPR, is shown in Fig. 1.

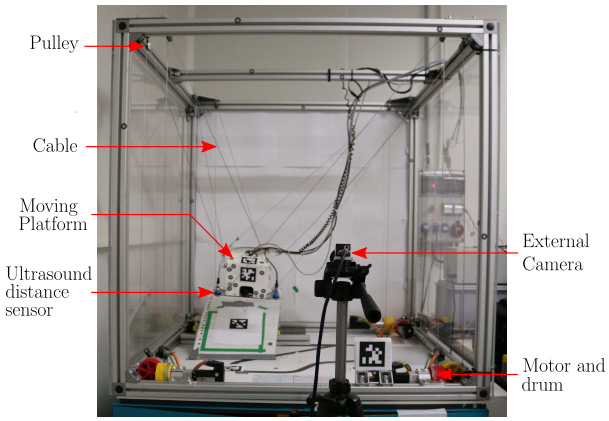

Fig. 1: ACROBOT, a CDPR located at IRT Jules Verne

This paper is organized as follows: Section 2 presents the two sensors and their kinematics modeling. The control law is recalled from [7] in Section 3. Section 4 focuses on the design of the stability criterion and Section 5 presents the numerical results of the stability analysis. Conclusions are drawn in Section 6.

2 Task definition

The CDPR considered in this paper is subject to a control law enabling its MP to perform a profile following task. This task can be divided into two subtasks:

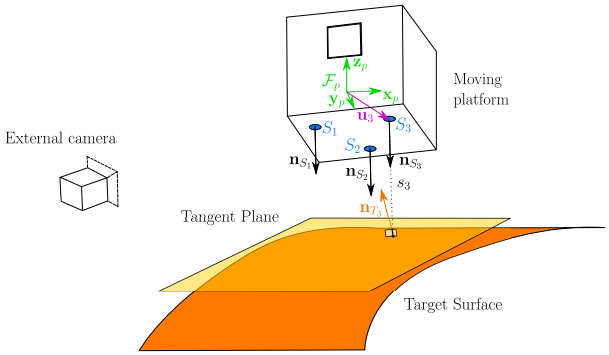

Fig. 2: Parametrization of the three distance sensors embedded on the MP and facing the target surface. The external camera observes the MP.

maintaining the MP parallel to the followed surface at a constant distance, denoted $\mathcal{T}_1$, and moving from a starting pose to a target pose along the profile, denoted $\mathcal{T}_2$. The control of the robot stems from sensor-based control and combines measurements provided by two types of sensors: an array of three distance sensors embedded on the MP, and an external camera located in front of the robot. The boarded sensors and the surface to follow are shown in Fig. 2.

2.1 Sensors

Distance sensors Three ultrasonic distance sensors are placed on the bottom of the MP, facing downwards along the z-axis of the MP frame $\mathcal{F}_p$, as shown in Fig. 2. Since all sensors are coplanar and their directions are parallel, for the MP to be locally parallel to the surface, the three sensors must return the same distance. The vector of distances measured by the sensors is denoted as $\mathbf{s} = [s_1, s_2, s_3]^T$, s_i being the distance measured by the ith sensor S_i. The time derivative of the measured distance vector, noted $\dot{\mathbf{s}}$, is then expressed as a function of the MP twist $\mathbf{v}_p$:

$$\dot{\mathbf{s}} = {}^p\mathbf{L}_1 \, \mathbf{v}_p \tag{1}$$

with $\mathbf{v}_p = [{\boldsymbol{\nu}_p}^T, {\boldsymbol{\omega}_p}^T]^T$ where $\boldsymbol{\nu}_p$ is the MP linear velocity vector and $\boldsymbol{\omega}_p$ is its angular velocity vector, expressed in $\mathcal{F}_p$. ${}^p\mathbf{L}_1$ is the interaction matrix of the distance sensors [12, 13]. Using a constant value of the interaction matrix corresponding to the desired configuration is a usual choice in sensor-based control [13]. The interaction matrix ${}^p\mathbf{L}_1$ thus only depends on the respective positions (x_i, y_i) of the distance sensors expressed in $\mathcal{F}_p$, and can be evaluated for the particular case $\mathbf{s} = \mathbf{s}^*$, where $\mathbf{s}^* = [s^*, s^*, s^*]^T$ and with $s^* = 0.2$ m the common reference distance so that the MP is locally parallel to the followed surface:

$${}^p\mathbf{L}_{1|\mathbf{s}=\mathbf{s}^*} = \begin{bmatrix} 0 & 0 & -1 & -y_1 & x_1 & 0 \\ 0 & 0 & -1 & -y_2 & x_2 & 0 \\ 0 & 0 & -1 & -y_3 & x_3 & 0 \end{bmatrix} \tag{2}$$

External camera The images acquired by the external camera are processed by an algorithm recognizing several AprilTags, placed on the MP as well as on the starting and target points of the trajectory. The relative pose of the reference frames attached to these April Tags is then estimated with regard to the camera frame $\mathcal{F}_c$. Then, this pose is expressed in the world frame $\mathcal{F}_w$, and, as for Pose-Based Visual Servoing (PBVS), the visual features are selected as:

$$\mathbf{s}_v = \begin{pmatrix} {}^w\mathbf{t}_p \\ \theta\mathbf{u} \end{pmatrix} \tag{3}$$

where ${}^w\mathbf{t}_p$ is the position vector of the MP expressed in $\mathcal{F}_w$ and $\theta\mathbf{u}$ is the axis-angle representation of the rotation matrix ${}^{p^*}\mathbf{R}_p$. The target pose is given by:

$$\mathbf{s}_v^* = \begin{pmatrix} {}^w\mathbf{t}_p^* \\ \mathbf{0}_3 \end{pmatrix} \tag{4}$$

where ${}^w\mathbf{t}_p^*$ is the position of the target AprilTag in $\mathcal{F}_w$. The interaction matrix ${}^w\mathbf{L}_2$ of these visual features can be found in [13]:

$${}^w\mathbf{L}_2 = \begin{bmatrix} \mathbf{I}_3 & -[{}^w\mathbf{t}_p]_\times \\ \mathbf{0}_3 & \mathbf{L}_\omega \end{bmatrix} \tag{5}$$

with $[{}^w\mathbf{t}_p]_\times$ the skew-symmetric matrix of ${}^w\mathbf{t}_p$. $\mathbf{L}_\omega$ can be approximated by $\mathbf{I}_3$, the (3×3) identity matrix. To express this matrix in $\mathcal{F}_p$, the adjoint matrix ${}^w\mathbf{V}_p$ is used [11]:

$${}^w\mathbf{V}_p = \begin{bmatrix} {}^w\mathbf{R}_p & [{}^w\mathbf{t}_p]_\times \, {}^w\mathbf{R}_p \\ \mathbf{0}_3 & {}^w\mathbf{R}_p \end{bmatrix} \tag{6}$$

The change of reference frame is then performed:

$${}^p\mathbf{L}_2 = {}^w\mathbf{L}_2 \, {}^w\mathbf{V}_p \tag{7}$$

This interaction matrix only depends on the estimated position and orientation of the MP in $\mathcal{F}_w$.

2.2 Fusion using the Gradient Projection Method

The fusion between the data from the external camera and the three distance sensors is performed with the GPM. In this method, a first main task is considered as a priority, while only the part of the second task compatible with the realization of the first one is retained [9].

Main task The main task $\mathcal{T}_1$ is selected from the distance sensor measurements, such that the task error $\mathbf{e}_1$ is given by:

$$\mathbf{e}_1 = \mathbf{s} - \mathbf{s}^* \tag{8}$$

The next step is to determine the Jacobian of the main task. As described above in Section 2.1, the time variation of the main task is related to the MP twist

$\mathbf{v}_p$ by (1). As the inputs of the low-level controller of the CDPR are the velocities $\dot{\mathbf{l}}$ of the m cable lengths, they are related to $\mathbf{v}_p$ by:

$$\dot{\mathbf{l}} = \mathbf{A}\ \mathbf{v}_p \tag{9}$$

where the forward Jacobian matrix $\mathbf{A}$ of the CDPR is given by [5]:

$$\mathbf{A} = \begin{bmatrix} \mathbf{u}_1 & \dots & \mathbf{u}_i & \dots & \mathbf{u}_m \\ \mathbf{b}_1 \times \mathbf{u}_1 & \dots & \mathbf{b}_i \times \mathbf{u}_i & \dots & \mathbf{b}_m \times \mathbf{u}_m \end{bmatrix}^T \tag{10}$$

where $\mathbf{u}_i$ are the cable direction unit vectors, pointing from the exit points (pulleys) of the CDPR to the anchor points placed on the MP, and where $\mathbf{b}_i$ are the position vectors of the anchors points, known from the platform design. All these vectors are expressed in $\mathcal{F}_p$. $\mathbf{u}_i$ vectors are calculated geometrically from the MP pose expressed in $\mathcal{F}_w$ using the straight and inelastic cable model [5].

Equations (1) and (9) can be combined to obtain:

$$\dot{\mathbf{e}}_1 = \mathbf{J}_1 \dot{\mathbf{l}} \tag{11}$$

where the Jacobian $\mathbf{J}_1$ of the main task is a $(3 \times m)$ matrix, given by

$$\mathbf{J}_1 = \mathbf{L}_1 \mathbf{A}^+ \tag{12}$$

with $\mathbf{A}^+$ the Moore-Penrose pseudo-inverse of $\mathbf{A}$.

Secondary task $\mathcal{T}_2$ consists in minimizing the error between the current and the desired MP poses, expressed in $\mathcal{F}_w$, and noted as follows:

$$\mathbf{e}_2 = \mathbf{s}_v - \mathbf{s}_v^* \tag{13}$$

From (7) and (9), its Jacobian is a $(6 \times m)$ matrix given by:

$$\mathbf{J}_2 = {}^w\mathbf{L}_2\ {}^w\mathbf{V}_p\ \mathbf{A}^+ \tag{14}$$

Similarly to (11), $\dot{\mathbf{e}}_2$ satisfies the following relationship:

$$\dot{\mathbf{e}}_2 = \mathbf{J}_2 \dot{\mathbf{l}} \tag{15}$$

3 Control strategy

In practice, the true Jacobians $\mathbf{J}_1$ and $\mathbf{J}_2$ can be subject to approximations, which is the case for the form given in (2), noise measurements, and calibration errors. The Jacobians used in the control scheme are thus different from the true ones and are denoted $\widehat{\mathbf{J}}$ in the following. The control law, pictured in Fig. 3 and performing the fusion described above, is detailed in [7]. It relies on the projection operator $\widehat{\mathbf{P}}_1$ on the kernel of the primary task given by:

$$\widehat{\mathbf{P}}_1 = \mathbf{I}_m - \widehat{\mathbf{J}}_1^+ \widehat{\mathbf{J}}_1 \tag{16}$$

The control law is expressed in terms of $\mathbf{e}_1$ and $\mathbf{e}_2$, with the gain ratio $r_\lambda = \lambda_2/\lambda_1$

$$\dot{\mathbf{l}} = -\lambda_1 \widehat{\mathbf{J}}_1^+ \ \mathbf{e}_1 - \lambda_1 (\mathbf{J}_2 \widehat{\mathbf{P}}_1)^+ (r_\lambda \mathbf{e}_2 - \mathbf{J}_2 \widehat{\mathbf{J}}_1^+ \mathbf{e}_1) \tag{17}$$

To simplify the notations, the term $\tilde{\mathbf{e}}_2 = r_\lambda \mathbf{e}_2 - \mathbf{J}_2 \widehat{\mathbf{J}}_1^+ \mathbf{e}_1$ and matrix $\widehat{\tilde{\mathbf{J}}}_2 = \mathbf{J}_2 \widehat{\mathbf{P}}_1$ are defined such that the control law has the simple form:

$$\dot{\mathbf{l}} = -\lambda_1 (\widehat{\mathbf{J}}_1^+ \ \mathbf{e}_1 + \widehat{\tilde{\mathbf{J}}}_2^+ \ \tilde{\mathbf{e}}_2) \tag{18}$$

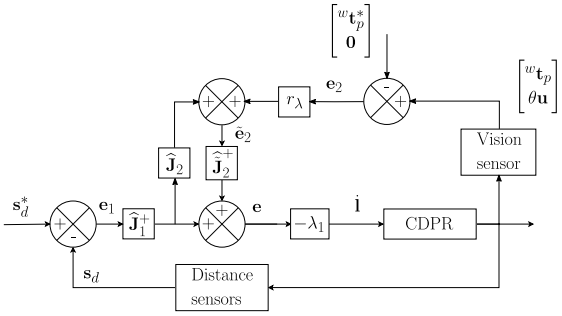

Fig. 3: Control scheme of the CDPR with the fusion of the distance and pose errors.

4 Stability criterion

The stability of the control scheme can be classicaly assessed using a Lyapunov stability analysis. Since the main task is of dimension three, the projection of the secondary task on the kernel of the main task causes the secondary task to lose three degrees of freedom. Hence, the stability of the control law cannot be assessed directly by considering $||\mathbf{e}_1||^2 + ||\mathbf{e}_2||^2$ as candidate Lyapunov function.

4.1 Secondary task error redefinition

To solve the analysis problem, a three-dimensional secondary task $\mathbf{e}_{2r}$ can be defined by projecting the six-dimensional secondary task $\mathbf{e}_2$ on the null space of $\mathbf{e}_1$, expressed in the MP frame. First, the projected error $\mathbf{e}_2^{'}$ is considered:

$$\mathbf{e}_2^{'} = {}^p\widehat{\mathbf{P}}_1 \ \mathbf{e}_2, \text{ with } {}^p\widehat{\mathbf{P}}_1 = \mathbf{I}_6 - \widehat{{}^p\mathbf{L}}_{1|\mathbf{s}=\mathbf{s}^*}^+ \widehat{{}^p\mathbf{L}}_{1|\mathbf{s}=\mathbf{s}^*} \tag{19}$$

Considering only the three non-zero terms of $\mathbf{e}_2^{'}$, the reduced error vector $\mathbf{e}_{2r}$ can be defined as:

$$\mathbf{e}_{2r} = \begin{bmatrix} {}^w x_p - {}^w x_p^* \\ {}^w y_p - {}^w y_p^* \\ \theta u_z \end{bmatrix} \tag{20}$$

The stacked vectors $\mathbf{e}_1$ and $\mathbf{e}_{2r}$ hence form a six-dimensional error. The corresponding stability problem can be assessed since the dimension of the variables

matches the number of DoF of the MP. The modified interaction matrix ${}^{p}\mathbf{L}_{2r}$ is then obtained by selecting the rows corresponding to the retained features and the corresponding modified matrices $\mathbf{J}_{2r}$ and $\tilde{\mathbf{J}}_{2r}$ are computed similarly by substituting $\mathbf{L}_2$ by $\mathbf{L}_{2r}$ in their definition. A modified control law follows:

$$\dot{\mathbf{l}} = -\lambda_1(\widehat{\mathbf{J}}_1^+ \ \mathbf{e}_1 + \widehat{\tilde{\mathbf{J}}}_{2r}^+ \ \tilde{\mathbf{e}}_{2r}) \tag{21}$$

4.2 Lyapunov stability criterion

By considering the reduced secondary task, the Lyapunov candidate function $\mathcal{L}$, strictly positive and continuously differentiable, is defined as:

$$\mathcal{L} = \frac{1}{2}||\mathbf{e}_1||^2 + \frac{1}{2}||\mathbf{e}_{2r}||^2 \tag{22}$$

Its time derivative is nothing but:

$$\dot{\mathcal{L}} = \mathbf{e}_1^T\dot{\mathbf{e}}_1 + \mathbf{e}_{2r}^T\dot{\mathbf{e}}_{2r} = \mathbf{e}_1^T\mathbf{J}_1\dot{\mathbf{l}} + \mathbf{e}_{2r}^T\mathbf{J}_{2r}\dot{\mathbf{l}} \tag{23}$$

Assuming the low level robot controller is able to perfectly apply the cable velocity vector computed by the control law (21), we obtain:

$$\begin{aligned}\dot{\mathcal{L}} = -\lambda_1 \Big[& \mathbf{e}_1^T\mathbf{J}_1\widehat{\mathbf{J}}_1^+\mathbf{e}_1 - \mathbf{e}_1^T\mathbf{J}_1\widehat{\tilde{\mathbf{J}}}_{2r}^+\widehat{\mathbf{J}}_{2r}\widehat{\mathbf{J}}_1^+\mathbf{e}_1 + r_\lambda\mathbf{e}_1^T\mathbf{J}_1\widehat{\tilde{\mathbf{J}}}_{2r}^+\mathbf{e}_{2r} \\ & + \mathbf{e}_{2r}^T\mathbf{J}_{2r}\widehat{\mathbf{J}}_1^+\mathbf{e}_1 + r_\lambda\mathbf{e}_{2r}^T\mathbf{J}_{2r}\widehat{\tilde{\mathbf{J}}}_{2r}^+\mathbf{e}_{2r} - \mathbf{e}_{2r}^T\mathbf{J}_{2r}\widehat{\tilde{\mathbf{J}}}_{2r}^+\widehat{\mathbf{J}}_{2r}\widehat{\mathbf{J}}_1^+\mathbf{e}_1 \Big]\end{aligned} \tag{24}$$

The previous equation can be expressed in a matrix form such that the Lyapunov candidate function derivative $\dot{\mathcal{L}}$ is expressed as:

$$\dot{\mathcal{L}} = -\lambda_1[\mathbf{e}_1^T\mathbf{e}_{2r}^T] \ \mathbf{\Pi} \begin{bmatrix}\mathbf{e}_1 \\ \mathbf{e}_{2r}\end{bmatrix} \tag{25}$$

which leads to the stability criterion $\mathbf{\Pi} > 0$ with:

$$\mathbf{\Pi} = \begin{bmatrix}\mathbf{J}_1(\mathbf{I}_m - \widehat{\tilde{\mathbf{J}}}_{2r}^+\widehat{\mathbf{J}}_{2r})\widehat{\mathbf{J}}_1^+ & r_\lambda\mathbf{J}_1\widehat{\tilde{\mathbf{J}}}_{2r}^+ \\ \mathbf{J}_{2r}(\mathbf{I}_m - \widehat{\tilde{\mathbf{J}}}_{2r}^+\widehat{\mathbf{J}}_{2r})\widehat{\mathbf{J}}_1^+ & r_\lambda\mathbf{J}_{2r}\widehat{\tilde{\mathbf{J}}}_{2r}^+\end{bmatrix} \tag{26}$$

In the ideal case, that is when the Jacobians used in the control scheme correspond to the real ones, *i.e.,* $\widehat{\mathbf{J}}_1 = \mathbf{J}_1$ and $\widehat{\tilde{\mathbf{J}}}_2 = \tilde{\mathbf{J}}_2$, it follows that $\mathbf{J}_1\tilde{\mathbf{J}}_{2r}^+ = \mathbf{0}_3$ and the expression of matrix $\mathbf{\Pi}$ becomes:

$$\mathbf{\Pi} = \begin{bmatrix}\mathbf{I}_3 & \mathbf{0}_3 \\ \mathbf{J}_{2r}\mathbf{J}_1^+ - \mathbf{J}_{2r}\tilde{\mathbf{J}}_{2r}^+\mathbf{J}_{2r}\mathbf{J}_1^+ & r_\lambda\mathbf{J}_{2r}\tilde{\mathbf{J}}_{2r}^+\end{bmatrix} \tag{27}$$

As expected, the resulting expression in the ideal case matches with the relationship already established in [10].

5 Stability analysis

The sign of the Lyapunov function derivative $\dot{\mathcal{L}}$ depends on the sign of the criterion $\mathbf{\Pi}$. If the criterion is positive definite, the derivative is negative for all input vectors, thus guaranteeing the stability of the control law. This sign depends on the quality of the estimation of a series of parameters. These are the position error of the exit points of the pulleys and the anchor points of the cables on the MP $\boldsymbol{\delta}\mathbf{a}_i$ and $\boldsymbol{\delta}\mathbf{b}_i$, the vision-based pose estimate error $\boldsymbol{\delta}^w\widehat{\mathbf{t}}_p$, the positionning error of the distance sensors in the platform reference frame $\boldsymbol{\delta}\widehat{\mathbf{L}}_{s,d}$, the relative orientation of the surface to follow with regard to the platform frame, given by the vectors $\mathbf{n}_{T_i}$, as well as the gain ratio r_λ. Since there is an infinity of combinations of poses and parameter values, the path $\mathcal{P}$ validated experimentally in [7] on the ACROBOT is chosen for this study. An analysis parameter by parameter is run to determine which ones have an important impact on the stability and which ones can be neglected. Then, a combined analysis using known parameter values is conducted to provide us with the expected stability domain of the robot during its standard behaviour. The analytical sign analysis of $\mathbf{\Pi}$ is rather complex, due the multiple interactions between the parameters. A numerical analysis is thus proposed. For this analysis, an initial angle between the MP and the tangent plane to the surface followed of 15° was retained.

CDPR geometrical parameters The precision of the CDPR geometry parameters $\mathbf{a}_i$ and $\mathbf{b}_i$ values has an impact on $\widehat{\mathbf{A}}$ and hence on $\mathbf{\Pi}$. Considering only errors in the estimation of these parameters along the path $\mathcal{P}$, the stability margin versus both $\mathbf{a}_i$ and $\mathbf{b}_i$ parameters is shown Fig. 4. The control law remains stable up to an error of 0.08 m for $\mathbf{a}_i$ and to 0.10 m for $\mathbf{b}_i$. The stability isocontours, *i.e.,* the lines where the lowest eigenvalue remains constant, closely follow the altitude profile of the path, hinting at a significant dependency on this parameter regarding the stability of the control law. For this experiment system, the accuracy of these parameters is respectively 0.01 m for $\delta\mathbf{a}_i$ and 0.008 m for $\delta\mathbf{b}_i$. Hence, the stability of the robot is not threatened by these errors.

Vision-based pose estimation The pose estimation impacts the stability since it is involved in the estimation of the robot Jacobian $\mathbf{A}$ and ${}^p\mathbf{L}_2$, necessary to compute the estimates of $\mathbf{J}_1$ and $\mathbf{J}_{2r}$. The impact of the position measurement bias resulting of a low image resolution is shown Fig. 5. However, this bias is not uniformly distributed along the three directions, and the estimated position error is larger along the depth of the image observed by the camera. The norm of the position error plotted in Fig. 5 was thus distributed accordingly. The impact of the orientation error about the three directions of $\mathcal{F}_p$ was computed along $\mathcal{P}$, and is represented for a central position in the robot cell in Fig. 7. In both cases, the accuracy of the pose-estimation, 70 mm for the position and 3 degrees for the orientation at worst, does not overshoot the stability limits. However, the resulting margin is lower than the one obtained for the CDPR geometrical parameters errors and pose-estimation errors have a larger stability impact.

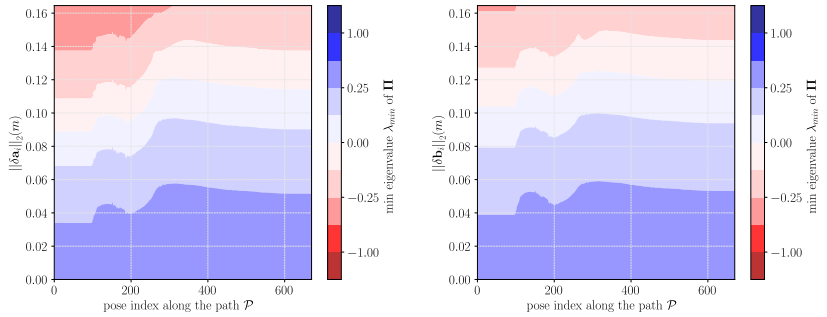

(a) Stability versus the norm of the exit point error $\delta\mathbf{a_i}$.

(b) Stability of the robot versus the norm of the anchor point error $\delta\mathbf{b_i}$.

Fig. 4: Stability of the robot along $\mathcal{P}$ versus the CDPR geometrical parameters.

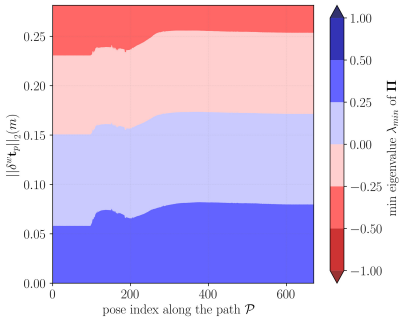

Fig. 5: Stability of the robot along $\mathcal{P}$ versus the position estimation error $\delta^w\mathbf{t}_p$

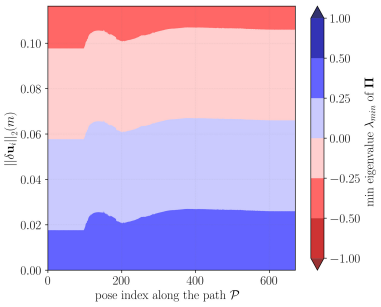

Fig. 6: Stability of the robot along $\mathcal{P}$ versus the norm of the sensor position error

Distance sensors positioning The position of the distance sensors with regards to the MP-frame is measured and these measured values x_i and y_i are used for computing matrix $\widehat{\mathbf{L}}_{s,d}$ (2). The impact of a measurement error on the stability of the control law is shown Fig. 6. From this figure, it is clear that the quality of such measurements significantly impacts the stability since the maximum norm of the error ensuring stability for these parameters is twice lower than for the parameters studied above. However, an adequate accuracy on these parameters can easily be achieved with a robust design of the MP or following a characterization of this MP. For ACROBOT, this accuracy is estimated to 1 mm.

Gain ratio Eventually, the gain ratio between the main task and the secondary task is also involved in the computation of the stability criterion $\mathbf{\Pi}_2$. The corresponding plot is not shown due to lack of space but the result obtained shows that this parameter cannot prevent the stability of the control law. However, the

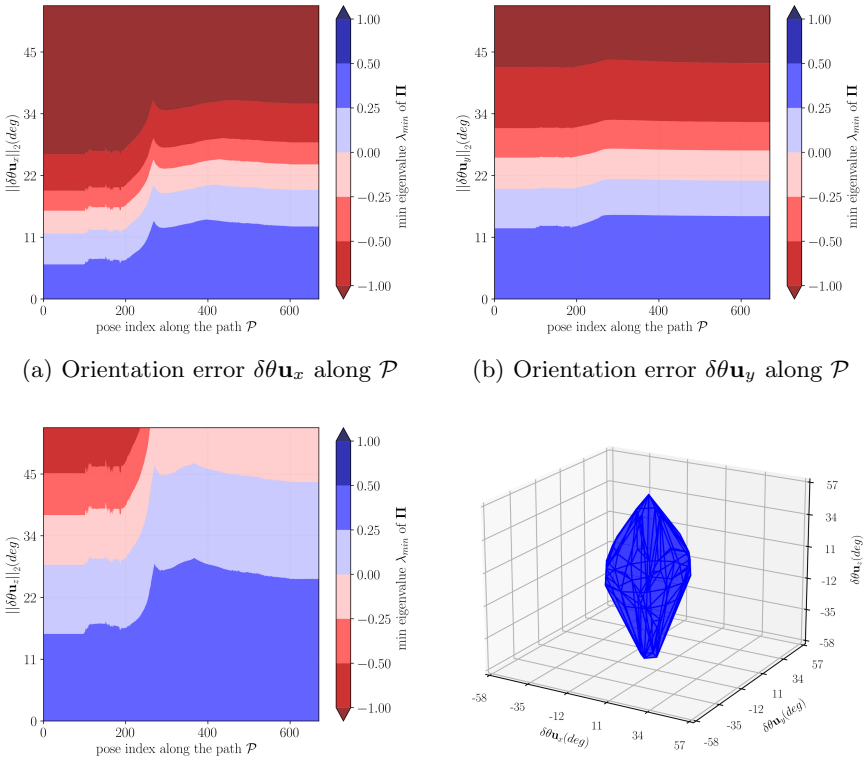

(a) Orientation error $\delta\theta\mathbf{u}_x$ along $\mathcal{P}$

(b) Orientation error $\delta\theta\mathbf{u}_y$ along $\mathcal{P}$

(c) Orientation error $\delta\theta\mathbf{u}_z$ along $\mathcal{P}$

(d) Stability isosurface of the robot at position [0, 0, 0.2]

Fig. 7: Stability of the robot versus the three components of the orientation estimation error $\delta\theta\mathbf{u}$

values below $r_\lambda = 0.25$ reduce the stability margin. Furthermore, no difference in stability has been noticed all along the path $\mathcal{P}$ for this parameter.

Combination of parameters To analyze the combination of these factors, another analysis is conducted, combining all the error sources. A series of 20.000 trajectories was run, selecting randomly the errors applied. Each of these parameters was assigned an error box whose side corresponds to its respective estimated accuracy. For each trajectory and for each parameter discussed above, a random vertex of the corresponding error box is selected. The distance measurements returned by the distance sensors are generated randomly with a Gaussian centered on $\mu = 0.2$ m and $\sigma = 0.025$. The distance difference between the three sensors generates an angle α between the normal $\mathbf{n}_S$ and the normal to the tangent plane

$\mathbf{n}_T$, equivalent to the angle between the plane $\mathbf{x}_p O_p \mathbf{y}_p$ and the tangent plane. The results of this analysis with regard to the angle α are presented Fig. 8.

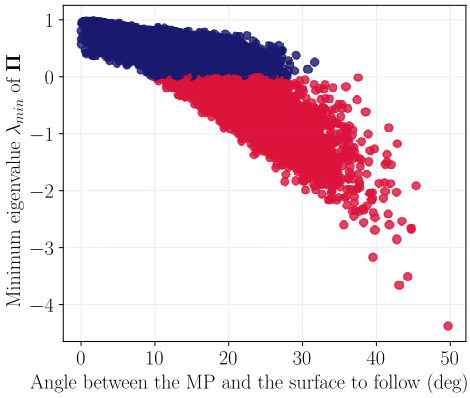

Fig. 8: Stability margin of the tested configurations versus orientation angle α. In blue: stable configurations and in red: unstable configurations.

When observing the minimum eigenvalues of the stability criterion versus the angle α, all configurations are stable when $\alpha \leq 11°$. However, after this threshold, the proportion of stable configurations decreases when the angle increases. No stable configurations were found when $\alpha \geq 33°$. This implies that an initial configuration of the system with α lower than 11° and that, while executing the two tasks, the tracking error with regard to the main task remains below 11° is a sufficient condition for the convergence of the system. On the tested trajectory $\mathcal{P}$, the orientation of the tracking error does not exceed 8°, and the stability of the control law with the measured parameter errors is thus ensured.

6 Conclusion

This paper proposed a stability analysis of a sensor-based control law for profile following using a CDPR. First, a stability criterion was derived, then a numerical parameter by parameter analysis was conducted, highlighting the most critical parameters that ensure the stability of the system. The most critical parameters are the coordinates of the distance sensor in the MP frame as well as the bias on the vision-based pose estimation. A combined analysis taking into account the most relevant parameters for various configurations of the robot was also presented. This analysis shows that all these configurations for the biases of the relevant parameters of the prototype ACROBOT are stable when the angle between the MP and the tangent plane to the target surface is smaller than 11°. A sufficient condition for the stability of the system on the initial configuration of the robot and on the tracking error hence results from this analysis. This implies that the response time of the main task must remain short so that

the moving MP during the trajectory following does not overshoot the stability angle threshold. While these results are specific to the ACROBOT prototype, the method is transferable. Stability domains of other CDPRs using the same control scheme can be computed similarly if the relevant parameters are given.

References

1. Pott, A. (2012). Influence of pulley kinematics on cable-driven parallel robots. In Latest Advances in Robot Kinematics (pp. 197-204). Springer, Dordrecht.
2. Mishra, Utkarsh A. et Caro, Stéphane. Mishra, U. A., and Caro, S. (2022). Forward kinematics for suspended under-actuated cable-driven parallel robots with elastic cables: A neural network approach. Journal of Mechanisms and Robotics, 14(4), 041008.
3. Schmidt, V. L. (2017). Modeling techniques and reliable real-time implementation of kinematics for cable-driven parallel robots using polymer fiber cables. Stuttgart: Fraunhofer Verlag.
4. Dallej, T., Gouttefarde, M., Andreff, N., Michelin, M., and Martinet, P. (2011, September). Towards vision-based control of cable-driven parallel robots. In 2011 IEEE/RSJ International Conference on Intelligent Robots and Systems (pp. 2855-2860). IEEE.
5. Zake, Z., Chaumette, F., Pedemonte, N., and Caro, S. (2019). Vision-based control and stability analysis of a cable-driven parallel robot. IEEE Robotics and Automation Letters, 4(2), 1029-1036.
6. Ramadour, R., Chaumette, F., and Merlet, J. P. (2014, May). Grasping objects with a cable-driven parallel robot designed for transfer operation by visual servoing. In 2014 IEEE International Conference on Robotics and Automation (ICRA) (pp. 4463-4468). IEEE.
7. Rousseau, T., Pedemonte, N., Caro, S. and Chaumette, F. (2023, May). Constant Distance and Orientation Following of an Unknown Surface with a Cable-Driven Parallel Robot. In 2023 IEEE International Conference on Robotics and Automation (ICRA). IEEE.
8. Nakamura, Y., Hanafusa, H., and Yoshikawa, T. (1987). Task-priority based redundancy control of robot manipulators. The International Journal of Robotics Research, 6(2), 3-15.
9. Siciliano, B. (1990). Kinematic control of redundant robot manipulators: A tutorial. Journal of intelligent and robotic systems, 3(3), 201-212.
10. Antonelli, G. (2009). Stability analysis for prioritized closed-loop inverse kinematic algorithms for redundant robotic systems. IEEE Transactions on Robotics, 25(5), 985-994.
11. Zake, Z., Chaumette, F., Pedemonte, N., and Caro, S. (2021, July). Control Stability Workspace for a Cable-Driven Parallel Robot Controlled by Visual Servoing. In International Conference on Cable-Driven Parallel Robots (pp. 284-296). Springer, Cham.
12. Samson, C., Espiau, B., and Borgne, M. L. (1991). Robot control: the task function approach. Oxford University Press, Inc.
13. Chaumette, F., Hutchinson, S., and Corke, P. (2016). Visual servoing. In Springer Handbook of Robotics (pp. 841-866). Springer, Cham.